JOURNAL OF SOLID STATE CHEMISTRY 87, 366–377 (1990)

Chemical Bonding and Electronic Properties in Antimony Chalcogenides

J. OLIVIER-FOURCADE,* A. IBANEZ,* J. C. JUMAS,* M. MAURIN,* I. LEFEBVRE,† P. LIPPENS,† M. LANNOO,† AND G. ALLAN†

*Laboratoire de Physicochimie des Matériaux Solides, URA D0407 CNRS, Université des Sciences et Techniques du Languedoc, Place E. Bataillon, 34060 Montpellier Cedex, France; and †Laboratoire de Physiques des Solides ISEN, U.A. 253 CNRS, 41 boulevard Vauban, 59046 Lille Cedex, France

Received January 4, 1990; in revised form April 5, 1990

The lone-pair antimony chalcogenides are investigated. A detailed qualitative classification of their properties is worked out. We show that the ^{121}Sb Mössbauer isomer shift increases with the covalent character of bonds and with the distortion of the local antimony environment. This is quantitatively explained by a tight-binding band-structure calculation. The lone-pair stereochemical activity also weakens with the forbidden band gap while the conductivity and the metallic character of bonds increase. © 1990 Academic Press, Inc.

Introduction

The search for new physical properties and the possibility of continuously varying already known properties led to the use of materials with more complex structures. For instance, the optical transmission of information—emission, transmission, detection signal processing—requires large variations in the electronic behavior of the corresponding materials. This also happens in high-temperature superconductors. Thus, an important general question concerns the nature and desired properties of the materials that have to be prepared for the technology of the future (*1*). For partial answers, one must systematically relate the electronic properties to the atomic structure. For this purpose one must find computational methods that permit the calculation of the band structure of complex materials with low symmetry and a large number of atoms per unit cell.

For such a general study, "lone-pair" elements represent quite an interesting family since they participate in the formation of a large number of atomic arrangements, resulting in a variety of electrical and optical properties (*2–5*). The existence of such diversity for a given family of compounds (chalcogenides), with the same central element (antimony), permits the determination of the principal factors for each type of property, as well as their connection with atomic structure.

Our aim here is to determine the links between the atomic structure and the electronic properties for lone-pair antimony chalcogenides. We also show that these can be summarized in terms of lone-pair effect.

0022-4596/90 $3.00

First (Section I), we present the relevant properties of systems containing lone-pair elements. Then (Section II) we detail the possible ways of classifying the compounds according to the nature of their bonds and the experimental results. Among these the Mössbauer parameters (the isomer shift δ and the quadrupolar splitting Δ), which provide information about the local electronic distribution, are examined in detail. Qualitative classifications are provided in Section III to show the relationships existing between the nature of the chemical bonding, the electronic properties, and the Mössbauer parameters. As the Mössbauer results seem to be reflective of the other parameters, we finally present a band structure and an isomer shift calculation for five specific systems (Section IV) which further allows the quantification of lone-pair behavior and its link to the atomic structure.

I. Why Study Lone-Pair Elements?

The electronic structure of a "pair" element like antimony ([Kr]: $4d^{10}5s^25p^3$) is a dominant factor in the formation of the many structural varieties in which it participates. In its lower oxidation state, Sb^{III}, it exhibits two different types of limiting behavior:

(i) it donates its p electrons to elements that have a higher electron affinity (halogens), leading to compact ionic structures with Sb^{3+} cations and Cl^- anions. These crystals have high symmetry and are mainly based on local octahedral coordination (*6*, *7*).

(ii) it shares its p electrons with elements of comparable electronegativity such as S, Se, Te. The bonds then have more or less covalent character (S, Se) or even metallic character (Te). The local atomic arrangement can be strongly (*8*) or weakly (*9*) distorted, as determined by a parameter called "the stereochemical activity of the nonbonded pair E."

The notion of "stereochemical activity" of the pair E is to be related to the loss of sphericity of the $5s^2$ electron distribution around the Sb atom. Although this electron pair does not participate in bonding, its properties are connected to the local atomic arrangement of Sb. Its stereochemical activity increases with the distortion of the local environment. Many studies have been devoted to this idea with the aim of elaborating general rules for the prediction of structural types in such molecules and compounds. Among these studies one can cite

—those of Gillespie and Nyholm (*10*) who have developed the VSEPR (Valence Shell Electron Pair Repulsion) theory which allows the prediction of molecular geometries from simple rules based on the piling up of bonding and nonbonding electron pairs.

—those of Galy *et al.* (*11*) showing that the volume occupied by a lone pair is often similar to that of an anion such as O^{2-} or F^-.

—those of Fourcade and Masherpa (*12*) who have extended the VSEPR theory to solid state by including the possibility of "long" bonds. The length of these secondary bonds, already mentioned by Alcock (*13*), is distinctly smaller than the sum of the Van der Waals radii; these occur in sterically significant directions.

The pair E is said to be very active when the coordination polyedra are small and the bonds are strongly covalent. This stereochemical activity of E decreases when the bonds are lengthened and the longer bonds are shortened, leading to larger and more symmetrical coordination shells (Fig. 1)

In practice, we have chosen to study here the antimony chalcogenides, chalcogenoiodides in the systems Sb_2X_3–SbI_3 (*14*), Sb_2Se_3–Sb_2Te_3 (*15*), A_2X–Sb_2X_3 (*16*), and SnX–SbI_3 (*14*) with A = Tl; X = S, Se, Te; I = iodine. In the isolated phases of the general formula Sb_bX_x, $A_aSb_bX_x$, $Sb_bX_xI_i$, and $Sn_aSb_bX_xI_i$ the change in nature of the elements A and X as well as variations in the

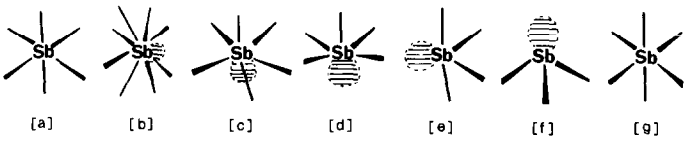

FIG. 1. Evolution of the Sb environment for increasing (b to f) stereochemical activity of the lone pair which is represented by the hatched orbital.

chemical composition defined by the values of a, b, x, and i modify of the local coordination around the central Sb atom. The structural modifications then correspond to changes in the nature of bonds from more or less ionic to covalent or metallic. These in turn correspond to substantial variations in electron states of the valence and conduction bands which are reflected in the densities of states and the values of the forbidden band gap.

II. Possible Classification of Chalcogenides

We have chosen to classify these materials according to the nature of their bonds, using the triangular diagram introduced in Ref. (*17*) whose corners correspond to the extreme situations: ionic—covalent—metallic (Fig. 2). This diagram rationalizes the synthesis of various physicochemical parameters which characterize strong chemical bonds. Obviously, there is no precise general definition of the nature of a bond but one can use several empirical classifications which have been quite helpful previously. We do this first but, in a second step, we also introduce experimental information relevant to such a classification.

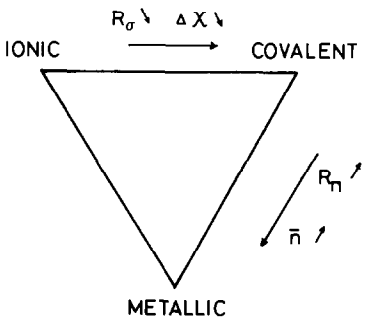

FIG. 2. Triangular diagram used to classify the materials according to the nature of their bond. Notations are the same as in the text.

A. Empirical Rules

There exist several ionicity scales which allow a satisfactory estimation of the iono-covalent character of the bonds in terms of the difference in electronegativity $\Delta\chi$ [Pauling (*18*), Phillips (*19*), Simmons and Bloch (*20*)]. However, this concept is incomplete since a small difference in electronegativity can correspond to the formation of metallic or covalent bonds; in the latter case the valence electrons are statistically involved in bonding with several atoms (*17, 21–23*).

One way of estimating the metallic character of a bond has been introduced by Mooser and Pearson (*24*) using the parameter $\bar{n}$ which is defined as the average principal quantum number of the atoms involved in the bond. The metallic character should increase with $\bar{n}$ since the overlap between atomic orbitals is more important. However, this criterion is still unsatisfactory since covalency is also related to strong overlap.

More recently two parameters R_σ and R_π have been introduced by Chelikowsky and Phillips (*25*) with the aim of estimating the

TABLE I

THEORETICAL VALUES OF VALENCE ORBITAL RADII IN ATOMIC UNITS (25)

	r_s	r_p
Sb	0.72	0.97
S	0.53	0.66
Se	0.59	0.76
Te	0.69	0.89

ionocovalent and covalometallic character. These parameters result from theoretical calculations (*20, 26*) of the "*s*" and "*p*" orbital radii (Table I); their physical meaning as discussed by Porte (*21*) can be summarized as follows:

$$R_\pi^{AB} = R_\sigma^A - R_\sigma^B = (r_s^A + r_p^A) - (r_s^B + r_p^B), \quad (1)$$

for a bond between atoms A and B, r_s and r_p being the s and p atomic radii. According to this definition R_σ increases with the size of an atom and also is a measure of its ability to capture available electrons. Thus R_σ^{AB} is maximum when the bond is strongly ionic and should characterize the ionocovalent character of a bond. The second parameter R_π^{AB} is defined as

$$R_\sigma^{AB} = R_\pi^A + R_\pi^B = (r_p^A - r_s^A) + (r_p^B - r_s^B). \quad (2)$$

The parameters R_σ^A and R_π^B measure the difference in s and p radii (related to the difference in s and p atomic energies) and can thus be used to characterize the degree of s–p hybridization. When R_π^{AB} is large (if A and B are heavy atoms) s–p hybridization is difficult and the bond will show metallic instead of covalent character, the opposite being true for small R_π^{AB}. Thus R_π^{AB} can be thought as a measure of the covalometallic character (*19*). However, care must be taken since this parameter does not take into account the possibility of having strong covalent bonds between pure p states, as are known to occur frequently.

B. Experimental Information for the Sb Chalcogenides

Important basic information is derived from X-ray diffraction on single crystals which permits the determination of the atomic positions. This provides all information about bond lengths, angles, and local atomic arrangements and determines the stereochemical role of E.

Among other tools, Mössbauer spectroscopy probes the local electronic environment of the central Sb atom. Such data can be summarized in terms of two parameters:

—The isomer shift δ which is a direct measure of the electron density of the Sb nucleus. It can be written in the form

$$\delta = \alpha(N)\,[|\Psi_a(O)|^2 - |\Psi_s(O)|^2], \quad (3)$$

which is the product of a nuclear factor, and an electronic factor that specifies the

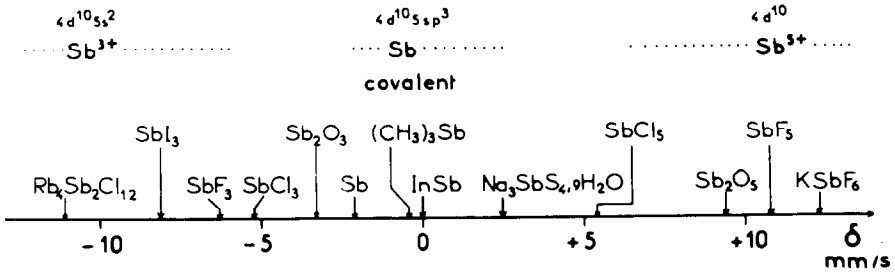

FIG. 3. Isomer shift scale with reference to InSb, for ^{121}Sb, recorded for different compounds.

difference in electron density at the Sb nucleus between the absorbing nucleus and the source. For Sb, α(N) is negative (*27*); an increase in δ corresponds to a decrease of the *s* electron density at the Sb nucleus. Thus, taking InSb as the source, values in the range $\delta < 0$ or $\delta > 0$ respectively characterize the tendencies for Sb to be in its III or V oxidation state, as shown in Fig. 3.

—The quadrupolar interaction Δ which can be expressed as

$$\Delta = eQV_{zz}\left(1 + \frac{\eta^2}{3}\right)^{1/2}, \qquad (4)$$

where eQ is the quadrupolar moment of the nucleus (negative for ^{121}Sb), V_{zz} is the principal component of the electric field gradient tensor, and η is the asymmetry parameter. Thus Δ is an indicator of the asymmetry of the electron distribution around the Sb atom. For instance, for the compounds SbX_3 (X = Cl, Br) (Fig. 4), Devort *et al.* (*28*) have shown that

$$V_{zz} \simeq (N_x - N_o)\left(\frac{3\cos\alpha}{\cos\alpha - 1}\right), \qquad (5)$$

where N_x and N_o respectively measure the electron populations along the Sb–X bond and in the lone-pair direction. Thus $\Delta \neq 0$ indicates an anisotropy of the electron distribution, $\Delta = 0$ corresponding to the fully isotropic case.

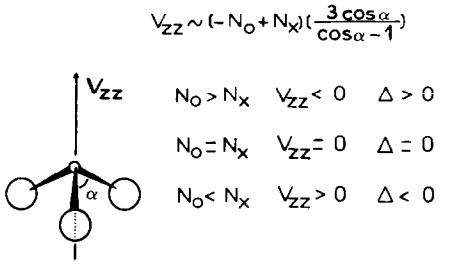

FIG. 4. SbX_3 (X = Cl, Br) molecules diagram used to realize the interpretation of the quadrupolar interaction (*28*).

TABLE II

PARAMETERS FOR THE CHALCOGEN X–Sb BOND

	Sb–S	Sb–Se	Sb–Te
$\Delta\chi$ (*18*)	0.6	0.5	0.2
$\bar{n}$	4	4.5	5
R_σ^{SbX}	0.5	0.34	0.11
R_π^{SbX}	0.38	0.42	0.45

Note. Notations are the same as in the text.

Other experimental quantities, such as the electrical conductivity σ versus temperature and the optical gap, E_g, have been recorded. They provide less direct information on the chemical bonding. Nevertheless, as will be shown below, they are related to the metallic character of bonds.

III. Discussion of Experimental Results

We now discuss the experimental trends in terms of the empirical parameters defined in the previous section. Table II lists the values of the different parameters $\Delta\chi$, $\bar{n}$, R_σ, and R_π versus the nature of the chalcogen element bonded to Sb. The corresponding

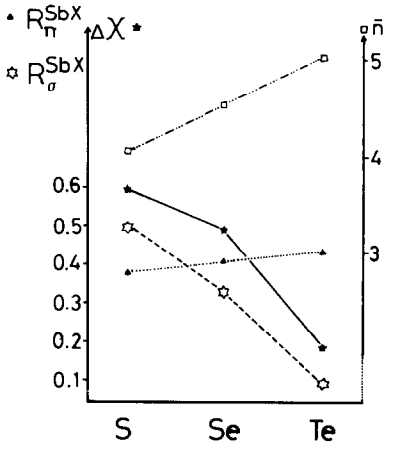

FIG. 5. Plot of R_σ, R, $\bar{n}$, and $\Delta\chi$ versus the chalcogen atom which is bonded to Sb atom.

TABLE III

MAIN PHYSICAL AND STRUCTURAL FEATURES

Compound	Sb local environment	Average length (Å) ⟨Sb–X⟩	⟨Sb–X⟩	⟨Sb–I⟩	⟨Sb–I⟩	E(Sb) activity	Mössbauer δ (mm/sec)	Δ	$\sigma V_{373\,K}$ $(\Omega cm)^{-1}$	E_g (eV)
SbI_3	3I + 3I	—	—	2.87	3.32	I	−8.10	0	10^{-9}	2.3
$Sn_2SbS_2I_3$	S + S + 6I + E	2.72	3.23	—	3.43	bA	−6.25	+11.2	10^{-8}	1.77
$Sn_2SbSe_2I_3$	Se + Se + 6I + E	2.82	3.34	—	3.45	bA	−6.11	+ 8.6	6.10^{-7}	1.22
$Sn_3SbSe_2I_5$		—	3.51	—	3.35	bA	−6.42	+ 9.9	6.10^{-7}	1.66
		2.91	—	—	3.42					
SbSI	S + 2S + 2I + 2I + E	2.40 2.69	—	3.11	3.80	A	−6.71	+ 6.9	$2.9.10^{-8}$	2.02
SbSeI	Se + 2Se + 2I + 2I + E	2.60 2.79	—	3.14	3.82	A	−6.93	+ 7.6	8.10^{-8}	1.63
Sb_2S_3	3S + 3S + E	2.33	3.34	—	—	A	−5.78	+ 7.8	$1.8.10^{-8}$	1.63
Sb_2Se_3	3Se + 3Se + E	2.66	3.24	—	—	A	−6.55	+ 6.8	3.10^{-7}	1.19
$TlSbS_2$	2S + 2S + S + E	2.44 2.77	3.70	—	—	vA	−3.96	+15.5	5.10^{-10}	1.77
Tl_3SbS_3	3S + 3S + E	2.43	3.60	—	—	vA	−2.95	+10.6	$1.6.10^{-7}$	1.80
SbTeI	Te + 2Te + 2I(+E)	2.83 2.95	—	3.22	3.82	≈I	−6.37	− 8.5	$3.5.10^{-5}$	1.45
Sb_2Te_3	3Te + 3Te	2.98	3.17	—	—	I	−6.74	− 4.2	$3.8.10^3$	0.21
Sb_2Te_2Se	3Te + 3Se	2.97	3.03	—	—	I	−7.27	− 3.9	$2.3.10^3$	≈0
Sb_2TeSe_2	3Te + 3Se	2.91	3.01	—	—	I	−7.33	− 3.9	$8.9.10^2$	≈0
	3Se + 3Se	2.88	2.98	—	—		−7.85	− 3.9		

Note. The stereochemical activity of the lone pair is noted; I: inactive bA: a bit active A: active vA: very active.

trends are pictured in Fig. 5. One finds that both $\Delta\chi_{Sb-X}$ and R_σ^{Sb-X} decrease with increasing atomic number of the chalcogen X. The ionicity thus decreases along the sequence S, Se, Te. On the other hand, both quantities $\bar{n}$ and R_π^{Sb-X} show the opposite trend. As seen in Section II this is probably related to an increase in metallic character.

Experimental data concerning the systems under study are summarized in Table III. The evolution in structure is shown by the large variety of possible local atomic arrangements around Sb, as shown in Fig. 6. All these can be described on the basis of an octahedron, which is undistorted for SbI_3 and Sb_2Te_3 (Figs. 6a and 6e), but is incomplete in the other cases. For instance, there is one missing atom at one edge of the octahedron for Sb_2S_3 and SbTeI (Fig. 6b), two for $TlSbS_2$ (Fig. 6c), or three for Tl_3SbS_3 (Fig. 6d). The stereochemical activity of the pair E is said to increase with the distortion of the octahedron. The manifestation of this activity occurs along a direction which, when associated with the normal bonding directions, defines polyhedra that are naturally described by the VSEPR theory (*10–12*): e.g., pyramids with square bases (Fig. 6b), bipyramids (Fig. 6c), and trigonal pyramids (Fig. 6d).

Information provided by Mössbauer spectroscopy which are important in the characterization of the activity of E can be discussed in terms of three limiting cases:

$-\delta$ minimal, $\Delta = 0$: the pair is inactive and spherically symmetric around Sb. The "*s*" electron density at the Sb nucleus is maximal, the bonds are predominantly ionic in character and the octahedra are weakly distorted (SbI_3).

$-\delta$ intermediate, $\Delta < 0$: this situation still corresponds to weakly distorted octahedra. Here the pair E remains inactive, but the "*s*" density decreases. One deals with a partially delocalized pair; the loss of "*s*" electrons might lead to anisotropy (since $N_0 < N_x$), such that $\Delta < 0$. The bonds now have metallic character (Sb_2Te_3).

$-\delta$ maximum, $\delta > 0$: this case occurs for strongly distorted octahedra. The pair E is said to be active, and the decrease in "*s*" electron density at the Sb nucleus is thought

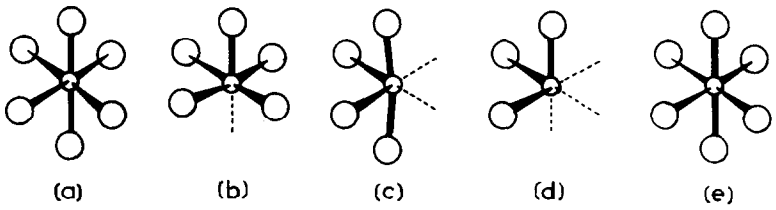

FIG. 6. Idealized Sb environment based on a perfect octahedron with N missing atoms. (a) and (e) $N = 0$; (b) $N = 1$; (c) $N = 2$; (d) $N = 3$.

to be due to a localization of the pair away from the nucleus. The fact that Δ is nearly positive indicates strong anisotropy, in agreement with the marked covalent character. All intermediate cases between this extreme situation and the two others are encountered (Figs. 6b, 6c, and 6d).

These trends in all electronic properties can be illustrated by selecting five typical cases (Fig. 7, Table III). Two extremes are, as discussed before, SbI_3 (weak conductivity, large gap, strong ionic character) and Sb_2Te_3 (high conductivity, zero gap, metallic character). Three intermediate situations are illustrated by $TlSbS_2$, Tl_3SbS_3, and SbTeI. These five examples will be discussed in detail in the next section with the use of band-structure calculations.

To summarize and classify the experimental results, with respect to the nature of their bonds, use the ternary diagram ionic–covalent–metallic (Fig. 8) whose characteristics are as follows:

—Within a family, and going from top to bottom, systems are classified as displaying increasing metallic character with in creasing $\bar{n}$ and R_π. The stereochemical activity of E weakens while the conductivity increases and the gap decreases. Only the systems in which one constituent is tellurium have a negative Δ, in agreement with the fact that this element has a tendency to form more metallic bonds than Se and S.

–In going from left to right one distinguishes between families. The presence of iodine atoms generally has the effect of increasing the ionic character of Sb–X bonds while the presence of thallium increases the covalent character. The isomer shift and the stereochemical activity of the pair E also increase with the covalent character.

—SbI_3 represents an extreme situation: it

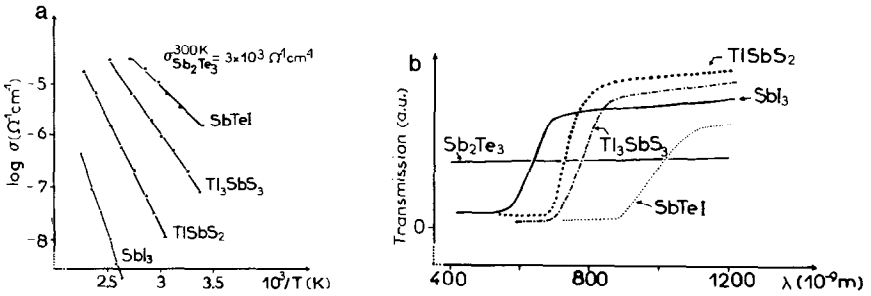

FIG. 7. Experimental values recorded for the five selected compounds: (a) electrical conductivity logarithm, versus the temperature inverse. (b) Optical transmission coefficient versus the wave length.

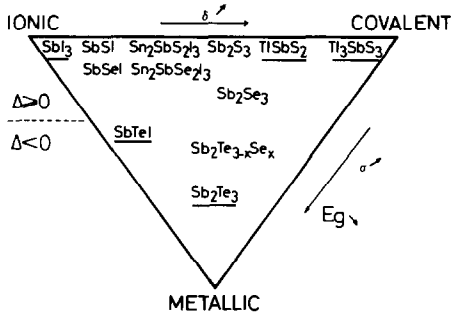

FIG. 8. Classification of iodides, chalcogenides and chalcogenoiodides in the ternary diagram. Underlined compounds have been selected for the calculation.

has the smallest δ, zero Δ, and very small conductivity. Moreover, iodine atoms increase the ionic character. Thus, this compound is located at the "ionic corner" which corresponds to an inactive pair E.

The ternary diagram of Fig. 8 is not completely coherent since the parameters δ, R_σ, $\Delta\chi$ and $\bar{n}$, R_π, σ, E_g are not perfectly correlated. But it has the advantage of summarizing the general links between bond character, electronic properties, and the stereochemical activity of the pair E. The Mössbauer parameters are helpful in classifying such properties.

Although the arguments developed in this section are very helpful for classification purposes, they remain too qualitative. In particular it is absolutely necessary to quantify the concept of stereochemical activity of the pair E and to show how it is manifested in the electronic structure. Toward this end we have performed a band-structure plus an isomer shift calculation for the five compounds selected earlier; these cover practically the entire surface of the triangle.

IV. Band Structure and Isomer Shift Calculation

The main problem with this family of materials is their complex atomic structure; the number of atoms per unit cell range from 6 to 24 for the five selected systems. For this reason we have chosen to apply here an empirical tight-binding approximation. This has several advantages:

(i) it is by far the simplest approach, especially from the computational point of view.

(ii) it has enjoyed much success in the last years at least for transition metals and tetrahedrally bonded semiconductors (*29, 30*).

(iii) it allows, in many cases, the derivation of very simple molecular models which approximate the actual band-structure and which lead to an understanding of the formation of compounds from the free atom states. However, such an approach can only describe the valence band and perhaps, the lowest conduction band, correctly.

In this procedure one writes the wave function of the system as a linear combination of atomic orbitals (LCAO approximation). These are then restricted to a minimal basis set built from orbitals belonging to the outer valence shell of the atoms (here one "*s*" and three "*p*" states). These atomic states are then assumed to be orthogonal (neglect of interatomic overlaps). The problem then reduces to a diagonalization of the Hamiltonian matrix in this atomic basis. However, two difficulties still arise:

(i) the theory deals with an infinite system,

(ii) one must determine the Hamiltonian matrix elements.

The first problem is solved by use of Bloch's theorem which exploits the translational periodicity of the crystal by performing a Fourier lattice sum for each orbital over the unit cells. Then for each vector $\vec{k}$, the size of the matrix is reduced here to $4N \times 4N$, where N is the number of atoms in the unit cell. The second difficulty is overcome by adopting an empirical relation for matrix elements between the atomic states in real space. Such a law has been established by Harrison (*30*) for tetrahedral semiconductors with the zinc blende structure. However, that law was restricted to nearest

neighbor interactions, while in our systems this concept must be generalized since we enounter a distribution of short distances. We have thus extended Harrison's formulation by writing the interatomic matrix elements between two atomic orbitals α and β as

$$H_{\alpha\beta} = \frac{\eta\alpha\beta}{d^2} \exp - 2.5\left(\frac{R}{d} - 1\right), \quad (6)$$

where the $\eta_{\alpha\beta}$ are the same as in Ref. (*31*), e.g.,

$$\eta_{ss} = 1.32 \quad \eta_{s\sigma} = -1.42 \quad (7)$$
$$\eta_{\sigma\sigma} = -2.22 \quad \eta_{\pi\pi} = -0.63,$$

and d is the shortest interatomic distance. The extension of the empirical law lies in the exponential term of Eq. (6), which allows inclusion of further neighbors with $R > d$ (the argument used in the exponential has been justified in Ref. (*33*)). However, we need to define a cut-off distance R_c beyond which the interactions are neglected; this is taken to be

$$R_c = 1.4\,(r_A + r_B), \quad (8)$$

where r_A and r_B are the atomic radii of atoms A and B calculated in Ref. (*34*). The factor 1.4 has been empirically chosen to obtain the best overall description for the five selected compounds. Finally, for the diagonal elements $H_{\alpha\alpha}$, we use the energies of the free atoms calculated by Herman and Skillman (*35*).

We now compare the theoretical band structure with experimental results. The predicted and observed values of the energy gap (in Table IV) are in good agreement, indicating that the lowest conduction bands are correctly described. The comparison with photoemission spectra shows that our calculations also correctly predict the number and position of the main peaks of the valence-density-of-states, as well as the valence band width (Fig. 9).

We then calculated the Mössbauer isomer shift which provides, as indicated earlier, experimental data on the stereochemical activity of the 5*s*(Sb) lone pair. This is intended to yield the order of magnitude of the "*s*" electron loss (i.e., 2 − Ns where Ns is the number of 5*s* electron on Sb nucleus) and delocalization. As shown by Eq. (3), this quantity is essential in the determination of δ. We obtain (Fig. 10a) a linear correlation between the measured δ and the computed values of 2 − Ns. The electron loss is always very small (less than 0.1 electron). Numerical verifications are provided in Ref. (*33*) by comparison of the experimental and calculated values of δ. Thus, the notion of strong or weak 5*s*(Sb) character is not an absolute one.

TABLE IV

PREDICTED GAP (E_g, p) COMPARED WITH THE EXPERIMENTAL ONE (E_g, e) IN ELECTRONVOLTS

Compound	E_g, p	E_g, e
SbI_3	2.40	2.30
Sb_2Te_3	0.14	0.21
SbTeI	1.32	1.45
$TlSbS_2$	1.73	1.77
Tl_3SbS_3	2.12	1.80

The main features of the band structures

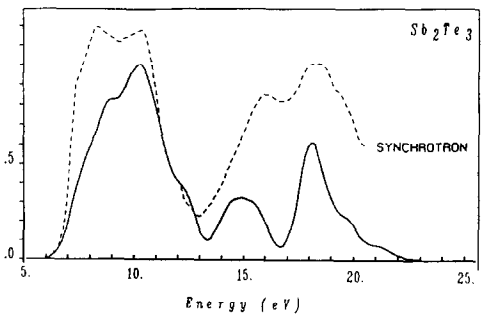

FIG. 9. Example of comparison between the photoemission results (*32*) (dashed line) and the valence-band density of states (solid line).

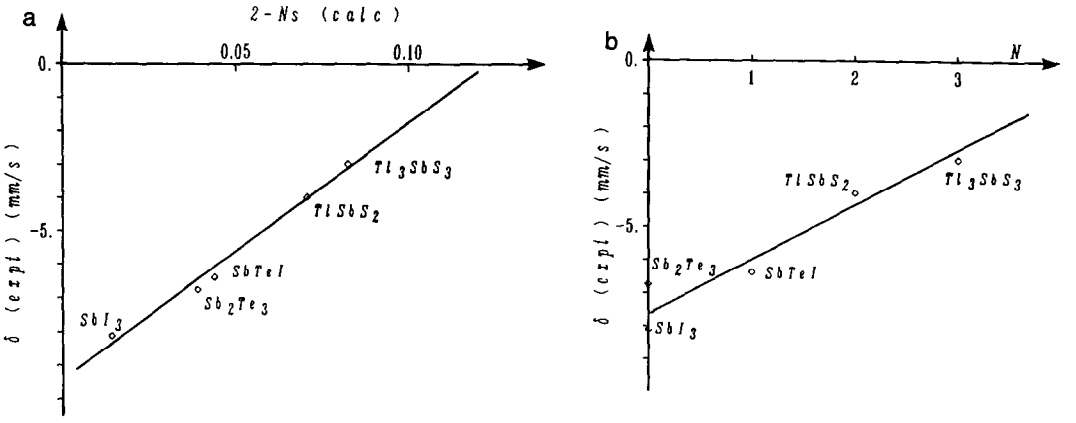

FIG. 10. Mössbauer isomer shift δ (a) vs 2 − Ns from tight-binding calculation; (b) vs N from molecular model.

can be found from a molecular model which also uses the tight-binding approximation. The model is based on suitable changes in the atomic orbital basis, such that the Hamiltonian matrix is dominated by some elements which correspond to the principal chemical bonds, the others being neglected. It describes the band structure as a set of highly degenerate molecular levels. Considering the five selected antimony chalcogenides, SbM_{6-N} molecules are constructed in the form of perfect octahedra (Fig. 6), where N of the possible sites are taken to be vacant (see Section III). A full explanation of each model calculation is given in a more detailed report (*33*) where we compare these to the computed density of states. This comparison shows that the main features are properly reproduced by the molecular models. Thus, these models correctly describe the qualitative trends in the chemical bonding.

To lowest order, one can simplify the level diagram model in the following manner for a SbM_{6-N} molecule: The basis functions are Φ_s, Φ_α ($\alpha = x, y, z$), the s and p states on the Sb atom, and χ_i, χ_j, the p states on M atoms. The p levels of the Sb and M atoms are taken as degenerate while the s level of the Sb atom is lower by about 10 eV, remaining uncoupled. For p coupling, two situations can occur for a given direction:

(i) the Sb atom has two neighbors. The Φ_α state couples to the antisymmetric state $(\chi_i - \chi_j)$, giving rise to a σ bonding state and σ^* antibonding one. The symmetrical $(\chi_i + \chi_j)$ 2 state remains at the p energy.

(ii) The Sb atom has only one neighbor. The Φ_α state couples to χ_i, giving rise again to σ and σ^* states, but with a smaller splitting. The level diagram is shown on Fig. 11. At this stage, one must note that the σ^*

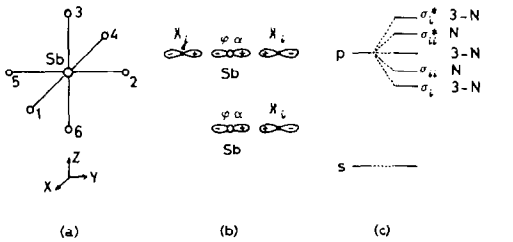

FIG. 11. (a) Idealized octahedron around Sb atoms. (b) Coupling between the Sb p orbital φ_α and the neighboring p orbitals, for the symmetrical situation (upper) and with one missing atom (lower). (c) Energy level diagram in the molecular model with the number of states per SbM_{6-N} unit.

states are empty, so that there are two 5*s* electrons on the Sb atom (Ns = 2).

We explain the trends in δ, in terms of a loss of 5*s*(Sb) electrons. This loss derives from the coupling between the Φ_s state and the σ^* empty levels. One can easily demonstrate that such coupling only exists in the second case. Thus, the total reduction in Ns (and then δ) is proportional to the number of units participating in this weak coupling (i.e., to the number N of missing atoms in the SbM_{6-N} unit). This is shown on Fig. 10b where the plot of experimental values of δ versus N represents a straight line. The other of magnitude of 2 − Ns is the same as those obtained with the full calculation (*33*). The spin-orbit coupling splits the bands which have a "*p*" character (σ and σ^* states) by a few tenths of an electron volt. This will not significantly change the 2 − Ns value because the loss involves second order interactions between the σ^* states and the Φ_s levels (lying 10 eV lower). We believe that the introduction of relativistic effects in the band-structure calculation is not necessary to explain the magnitude of the lone-pair loss. The very important point is our demonstration that, as shown in the previous classification (Section IV), the Mössbauer isomer shift is related to the local environment of Sb atoms.

Conclusion

We have discussed the relations existing between the atomic structure, the physical properties (electrical conductivity σ, optical band gap E_g), and the Mössbauer parameters for the lone-pair antimony chalcogenides. A qualitative classification of these systems has demonstrated the importance of the lone-pair effect. Its activity weakens with the gap while the conductivity increases.The quadrupolar splitting becomes negative when the metallic character increases. The isomer shift increases with the covalent character and with the distortion of the octahedral antimony environment. Thus, tight-binding calculations can explain the link between the lone-pair activity and the local distortion. These calculations also show that the lone-pair loss is always less than 0.1 electron. In conclusion, the lone-pair behavior as measured by Mössbauer spectroscopy is an important element for the understanding of the properties of these chalcogenides.

References

1. C. H. L. Goodman, *Mater. Res. Bull.* **20,** 237 (1985).
2. B. Roy, B. R. Chakraborty, R. Bhattacharya, and A. K. Dutta, *Solid State Commun.* **25,** 617 (1978).
3. H. T. Langhammer, M. Stordeur, H. Sobotta, and V. Riede, *Phys. Status Solidi* B **109,** 673 (1982).
4. K. Itoch and H. Matsunaga, *Z. Kristallogr.* **152,** 309 (1980).
5. A. Ibanez, J. Olivier-Fourcade, J. C. Jumas, E. Philippot, and M. Maurin, *Z. Anorg. Allg. Chem.* **540/541,** 106 (1986).
6. D. R. Schroeder and R. A. Jacolson, *Inorg. Chem.* **12,** 210 (1973).
7. J. Trotter and T. Zobel, *Z. Kristallogr.* **123,** 67 (1966).
8. P. Bayliss and W. Nowacki, *Z. Kristallogr.* **135,** 308 (1972).
9. T. L. Anderson and H. R. Krause, *Acta Crystallogr., Sect. B* **30,** 1307 (1974).
10. R. J. Gillespie and R. Nyholm, *Q. Rev. Chem. Soc.* **11,** 339 (1957); R. J. Gillespie, "Molecular Geometry," series in Inorganic Chemistry, Van Nostrand–Reinhold, Princeton NJ (1972); J. F. Sawer and R. J. Gillespie, "Progress in Inorganic Chemistry" (S. J. Lippard, Ed.), Vol. 34, p. 65, Wiley–Interscience, New York (1986).
11. J. Galy, G. Meunier, S. Anderson, and A. Astrom, *J. Solid State Chem.* **13,** 142 (1975); J. Galy and R. Enjalbert, *J. Solid State Chem.* **44,** 1 (1982).
12. R. Fourcade and G. Masherpa, *Rev. Chim. Minér.* **15,** 295 (1978).
13. N. W. Alcock, *Adv. Inorg. Chem. Radiochem.* **2,** 15 (1972).
14. A. Ibanez, J. C. Jumas. J. Olivier-Fourcade, and E. Philippot, *Rev. Chim. Minér.* **21,** 344 (1984).
15. A. Andriamihaja, A. Ibanez, J. C. Jumas, J. Olivier-Fourcade, and E. Philippot, *Rev. Chim. Minér.* **22,** 357 (1985).

16. J. C. JUMAS, J. OLIVIER-FOURCADE, N. REY, AND E. PHILIPPOT, *Rev. Chim. Minér.* **22,** 651 (1985).
17. J. LIVAGE, *La Recherche* **11,** 1272 (1980).
18. L. PAULING, "The Nature of the Chemical Bond and the Structure of Molecules and Crystals," Cornell University, New York (1960).
19. J. C. PHILLIPS, *Solid State Commun.* **22,** 549 (1977).
20. G. SIMMONS AND A. N. BLOCH, *Phys. Rev. B* **7,** 2754 (1973).
21. L. PORTE, *J. Solid State Chem.* **46,** 64 (1983).
22. G. LUCOVSKY AND R. M. WHITE, *Phys. Rev. B* **8,** 666 (1973).
23. H. KREBS, "Fundamentals of Inorganic Crystal Chemistry," McGraw–Hill, London (1968).
24. E. MOOSER AND W. B. PEARSON, *Acta Crystallogr.* **12,** 1015 (1959).
25. J. R. CHELIKOWSKY AND J. C. PHILLIPS, *Phys. Rev. B* **17,** 2453 (1978).
26. G. SIMMONS, *J. Chem. Phys.* **55,** 756 (1971); *Chem. Phys. Lett.* **12,** 404 (1971); *Chem. Phys. Lett.* **18,** 315 (1973).
27. J. G. STEVENS AND S. L. RUBY, *Phys. Lett. A* **32,** 91 (1970).
28. J. P. DEVORT, J. P. SANCHEZ, J. M. FRIEDT, AND G. K. SHENOY, *J. Phys. C* **6,** 1235 (1974).
29. J. FRIEDEL "The Physics of Metals" (J. M. Ziman Ed.), Cambridge Univ. Press, London/New York (1969).
30. W. A. HARRISON, Electronic Structure and Properties of Solids," Freeman, San Francisco (1980).
31. W. A. HARRISON, *Phys. Rev. B* **24,** 5885 (1981).
32. M. R. THULER, R. L. BENHOW, AND Z. HURYCH, *Chem. Phys.* **21,** 265 (1982).
33. I. LEFEBVRE, M. LANNOO, G. ALLAN, AND L. MARTINAGE, *Phys. Rev. B* **38,** 8593 (1988).
34. E. CLEMENTI, R. L. RAIMONDI, AND W. P. REINHARDT, *J. Chem. Phys.* **47,** 1300 (1967).
35. F. HERMAN AND S. SKILLMAN, "Atomic Structure Calculations," Prentice–Hall, Englewood Cliffs, NJ (1963).